Managing the Dynamics of a Harmonic Potential Field-Guided Robot in a Cluttered Environment

Ahmad A. Masoud, *Member, IEEE*

Abstract—This paper demonstrates the ability of the harmonic potential field (HPF) planning method to generate a well-behaved constrained path for a robot with second order dynamics in a cluttered environment. It is shown that HPF-based controllers may be developed for holonomic, as well as nonholonomic, robots to effectively suppress the effect of inertial forces on the robot's trajectory while maintaining all the attractive features of a purely kinematic HPF planner. The capabilities of the suggested navigation controller are demonstrated using simulation results for the holonomic and nonholonomic cases.

Index Terms—Intelligent control, nonholonomic robots, trajectory generation.

I. INTRODUCTION

A TRAJECTORY generator is an essential component of almost any automated industrial process [1]–[4]. A trajectory may be generated using a device called a planner. A planner is an interface between an operator and a servo process, whose function is to interpret the commands and constraints on the process behavior within the confines of its environment. The output of a planner is a context-sensitive, admissible, and goal-oriented sequence of action instructions, whose execution by the process actuators of motion produces a behavior that yields to the commands and constraints set by the operator. To function in this capacity, a planner has to carry out several tasks such as the following: changing the operator-centered format of the command and constraints on operation to a process-centered format. A planner must also act as a knowledge amplifier, augmenting the partial information supplied by the operator to the minimum level needed by the process to execute the supplied task in the specified manner.

The aforementioned task is by no means simple, particularly when servo processes with general dynamics are considered. Many of the practical aspects needed to construct planners that have a reasonable chance of success operating in a realistic environment are still open research problems. Understandably, the literature abounds with techniques and approaches for tackling this problem [5], [6]. Despite the diversity of planning methods, they may be divided into two classes: a class that separates a planner into two modules: one is called the high-level controller (HLC), and the other is called the low-level controller (LLC). The first is responsible for converting the command, constraints on process behavior, and environment feed into a desired behavior which the process must find a way to actualize if the task is to be accomplished (a know-what-to-do guidance signal). On the other hand, the second module determines what actions the process actuators of motion should release in order to actualize the desired behavior (a know-how-to-do control signal). Although this division of role in building planners is widely accepted by researchers in the area, it is believed to be a source of several problems. It is well known in practice that processes using the HLC–LLC paradigm are relatively slow. Incompatibilities between the guidance and control signals could lead to unwanted artifacts in the behavior and undesirable control effort that consumes too much energy or put too much strain on the actuators. Jointly designing the guidance and control modules is expected to yield a simpler and more efficient planner compared to a design that treats the two modules separately.

Simultaneous consideration of the guidance and control signals in the design of a planner is a challenging task. Whereas limited success was achieved in designing controllers that can incorporate simple avoidance regions with convex geometry in sate space [7], [8], imposing general nonconvex avoidance regions in the state space of a dynamical system is difficult [9], [10]. The task is further complicated when the state space constraints have to be implemented along with constraints in the control space, as is the case with dynamical nonholonomic systems.

Instead of using the relatively simple two-tier approach to planner design or the excessively complex joint state space control space approach, an approach in the middle is adopted. Here, the capabilities of a carefully selected planner that can only generate a guidance signal (i.e., deals only with the kinematic aspects of motion) are augmented to generate also the needed control signal. The guidance field from the kinematic planner is left unchanged. However, instead of the control component of the planner being designed to enforce strict compliance of motion with the guidance field, we only require that the control component strongly discourages motion from deviating from the course set by the guidance field. In its attempt to force compliance, the first approach injects too much energy into the system. This is expected to cause considerable transients in the response and an excessively high control effort. On the other hand, the passive nature of the suggested approach is highly unlikely to cause such problems.

As far as this paper is concerned, the extremely rich variety of kinematic motion planners may be categorized in one of

The author is with the Electrical Engineering Department, King Fahd University of Petroleum and Minerals, Dhahran 31261, Saudi Arabia (e-mail: masoud@kfupm.edu.sa).

two classes: path tracking and goal seeking planners. A path tracking planner provides a sequence of guidance instructions that mark one and only one path from an initial state to a target state. If an unexpected event occurs, throwing the state away from the guidance path, it must find its way back to the path in order to proceed to the target. On the other hand, a goal seeking planner supplies a guidance instruction at every possible state that the system may exist in. Therefore, a disruption caused by an influence external to the system will not cause a halt in the effort to drive the state closer to the target. For reasons that will become clearer later in the paper, goal seeking planners will be adopted in this paper. In particular, an efficient type of goal seeking planners known as harmonic potential field (HPF) planners will be used.

This paper is organized as follows. Section II provides a background of the HPF approach. Section III suggests a method for adapting the HPF method to deal with dynamic holonomic systems. Section IV tackles the dynamic nonholonomic HPF case. Conclusions are discussed in Section V.

II. HPF APPROACH—BACKGROUND

The microelement which an HPF planner utilizes for guiding the state of a system is a multidimensional vector attached to a specific point in state space. This element simply tells the system along which direction it should proceed if it is located at that state. A dense collective of theses vectors is induced using a surface (a potential field) along with a vector partial differential operator to fully cover the area of interest in the state space of the system (the workspace Ω). A group structure is then induced on this collective to generate a macrotemplate with a structure encoding the guidance information that the process needs to execute. The action selection mechanism that the approach utilizes for generating the structure is in conformity with the artificial life method [11]. The HPF approach offers a solution to the local minima problem faced by the potential field approach that Khatib suggested in [12]. It was simultaneously and independently proposed by several researchers [13]–[16] of whom the work of Sato in 1987 may be regarded as the first on the subject [17]. An HPF is generated using a Laplace boundary value problem (LBVP) configured using a properly chosen set of boundary conditions. There are several settings that one may use for an LBVP in order to generate a navigation potential [18]–[20]. Each one of these settings possesses its own distinct topological properties [14]. An example of an LBVP that is configured using the homogeneous Neumann boundary conditions is shown as follows:

$$\nabla^2 V(x) = 0, \qquad x \in \Omega \qquad (1)$$

subject to

$$V(x_s) = 1 \qquad V(x_T) = 0 \qquad \frac{\partial V}{\partial n} = 0, \qquad x = \Gamma$$

where Ω is the workspace, Γ is its boundary, $\mathbf{n}$ is a unit vector normal to Γ, x_s is the start point, and x_T is the target point.

The trajectory to the target $(x(t))$ is generated using the HPF-based gradient dynamical system

$$\dot{x} = -\nabla V(x), \qquad x(0) = x_0 \in \Omega. \qquad (2)$$

The generated trajectory is guaranteed to

$$\lim_{t \to \infty} x(t) \to x_T, \qquad x(t) \in \Omega.$$

Harmonic functions have many useful properties [21] for motion planning. Most notably, a harmonic potential is also a Morse function and a general form of the navigation function suggested in [24]. The HPF approach may be configured to operate in a model- and/or sensor-based mode. It can also be made to accommodate a variety of differential and state constraints [20]. The HPF approach is also very large scale integration (VLSI) friendly. Several VLSI chips were built to implement the HPF approach for fast trajectory generation [22], [23]. It ought to be mentioned that the HPF approach is only a special case of a much larger class of planners called evolutionary PDE-ODE motion planners [18].

Fig. 1 shows the guidance fields and paths generated by a special type of HPF planners [20] called nonlinear anisotropic HPF planner (NAHPF). In addition to enforcing regional avoidance constraints, NAHPF planners can also enforce directional constraints.

The results in Fig. 1 are for a kinematic planner, where the agent being guided is assumed to be a massless point. Assigning mass to the point robot totally changes the nature of the planning task. Here, the planner must find the x and y force components which, if applied to the point mass, yield a trajectory similar to the one shown in Fig. 1. One way to generate the control signal is to treat the gradient guidance field as a driving force augmented with linear viscous damping force having a coefficient B [25]. For a 1-kg mass, the system equation is as follows:

$$\begin{bmatrix} \ddot{x} \\ \ddot{y} \end{bmatrix} = -B \cdot \begin{bmatrix} \dot{x} \\ \dot{y} \end{bmatrix} - \begin{bmatrix} \partial V/\partial x \\ \partial V/\partial y \end{bmatrix}. \qquad (3)$$

Unfortunately, the provably correct properties of the kinematic planner can no longer be guaranteed. Fig. 2 shows the kinodynamic planner with $B = 0.2$ for a 1-kg point mass. As can be seen, the avoidance constraints failed, and collision with the walls of the room did occur despite the fact that the initial speed is zero.

III. HOLONOMIC CASE

Increasing the coefficient of viscous damping (B) may appear as the straightforward solution to the problem. Fig. 3 shows that increasing B decreases the transients in the trajectory induced by the inertial forces. As demonstrated, a high enough B has the ability to drive the spatial component of the dynamic trajectory arbitrarily close to the kinematic trajectory, hence improving the chance of the planner to enforce the spatial constraints. The price to be paid for adopting such a simple solution is making the system impractically slow.
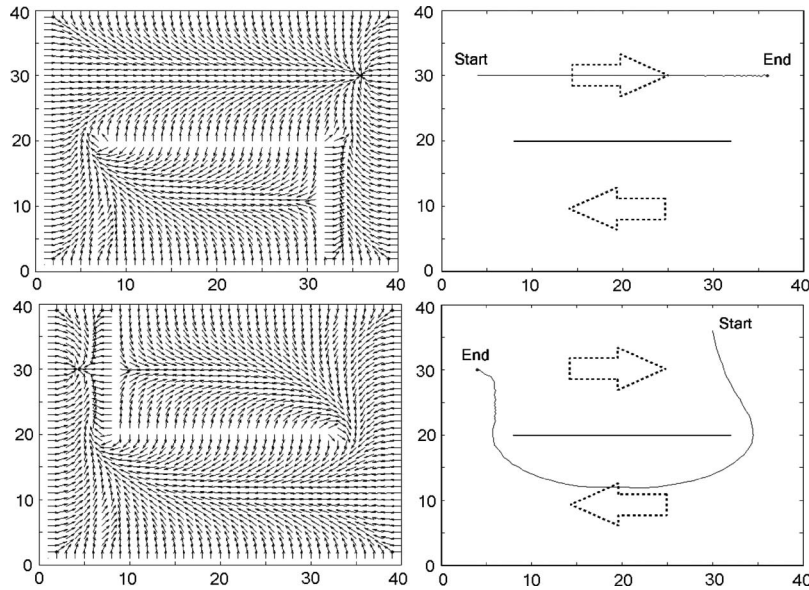
Fig. 1.   Output from a directional sensitive kinematic HPF planner.
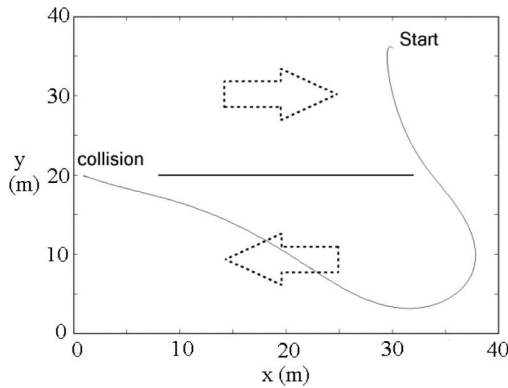
Fig. 2.   Inertial forces could lead to constraint violation.

A damping component that is proportional to velocity exercises omnidirectional attenuation of motion regardless of the direction along which it is heading. This means that the useful component of motion marked by the direction along which the goal component of the gradient of the artificial potential is pointing is treated in the same manner as the unwanted inertia-induced noise component of the trajectory. These two components should not be treated equally. Attenuation should be restricted to the inertia-caused disruptive component of motion, whereas the component in conformity with the guidance of the artificial potential should be left unaffected (Fig. 4). A damping force that takes the aforementioned components into consideration is as follows:

$$ u_d = -B_d \cdot \left[(n^t \dot{x})n + \left(\frac{u_g^t}{|u_g|} \cdot \dot{x} \cdot \Phi(-ug \cdot \dot{x}) \frac{u_g}{|u_g|} \right) \right] \quad (4) $$

where **n** is a unit vector orthogonal to u_g, u_g is the guidance force which, for the harmonic potential case, is chosen as $ug = -\nabla V$, u_d represents the damping force, B_d is a constant, and $\Phi()$ is the Heaviside step function. This force is given the following name: nonlinear anisotropic damping force (NADF).

It ought to be mentioned that u_g is the null space of NADF because impedance to motion, by design, is zero when the motion is fully aligned with u_g.

The NADF coefficient (B_d) is very easy to tune. Because, by design, the component of motion in conformity with the guidance field is in the null space of NADF, B_d may be set arbitrarily high to attenuate the disruptive competent caused by the robot's inertia. This may be done with no danger of slowing down the robot. The previous example is repeated using NADF. A high B_d of 2.5 is used. The trajectory is shown in Fig. 5, and the control forces are shown in Fig. 6. The spatial trajectory is well behaved, and a settling time (T_S) of 14 s is obtained. Despite the fact that the coefficient of NADF is two times and a half higher than the linear damping force coefficient used in Fig. 3, the system with NADF is more than five times faster.

NADF and linear viscous damping exhibit fundamentally different behavior as far as convergence is considered. The settling time for the point mass example is drawn in Fig. 7 as a function of the linear viscous friction coefficient (B). As can be seen, the T_S–B relation is convex with one value for B corresponding to a global minimum of T_S. This is expected because, for low B, high oscillations will prevent motion from quickly settling in the 5% zone around the target. On the other hand, a high value for B reduces the oscillations by slowing down the response, delaying the entrance to the 5% zone.

The relation between T_S and the coefficient of NADF (B_d) is a rapidly and strictly decreasing one (Fig. 8). Similar to the linear case, for a low value of B_d, high oscillations will prevent the quick capture of the trajectory in the 5% zone around the target. As the value of B_d increases, NADF, by design, only impedes the component of motion along the coordinate field tangent to the gradient guidance field. This component does not contribute to convergence, and it only causes delay in reaching the target. Because NADF attenuates this and only this component of motion, leaving the motion along the gradient field unaffected, the delay in reaching the target drops as B_d increases, yielding a strictly decreasing profile of the T_S–B_d curve.
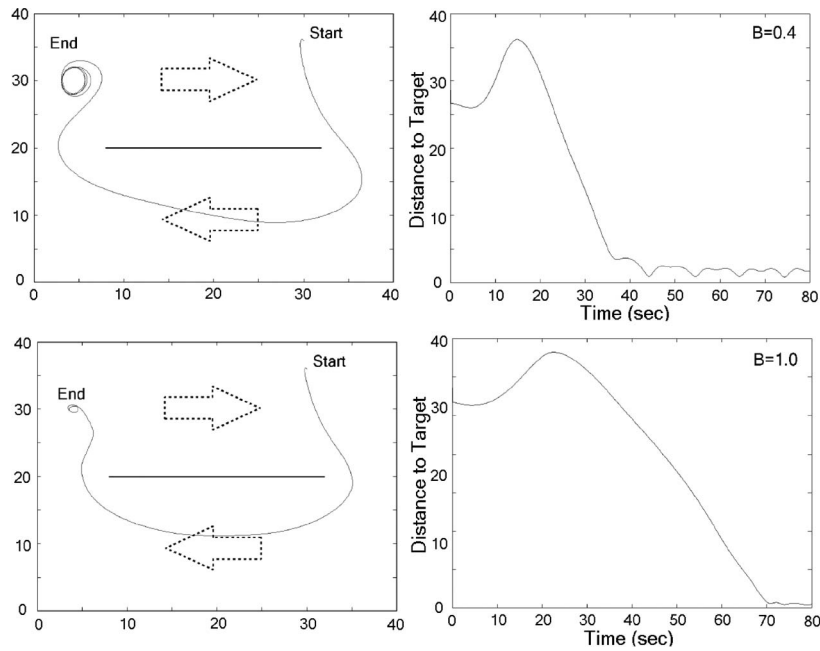
Fig. 3.   Increasing B reduces transients but slows down motion.
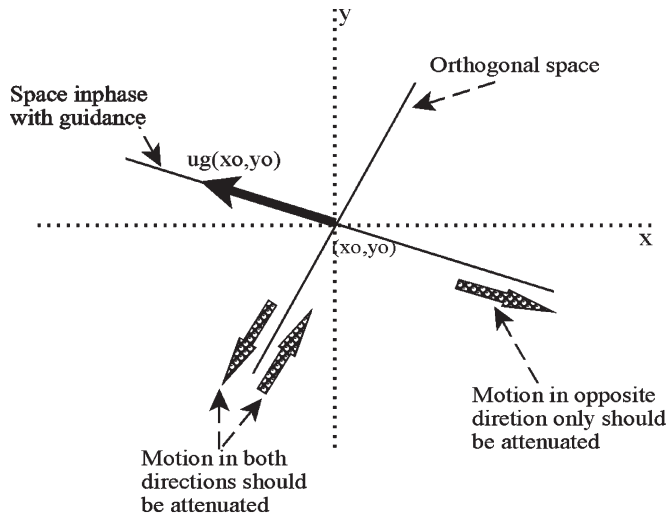
Fig. 4.   NADF.
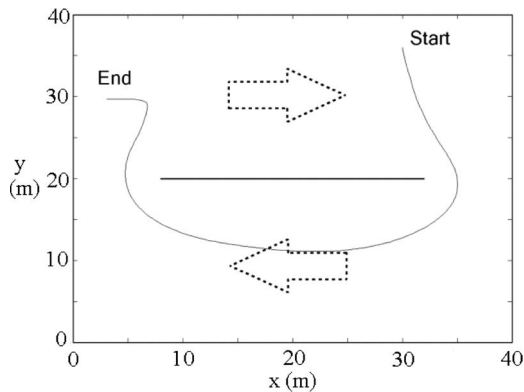
Fig. 5.   Trajectory for NADF; $B_d = 2.5$.

Fig. 6.   Control signal corresponding to Fig. 5.
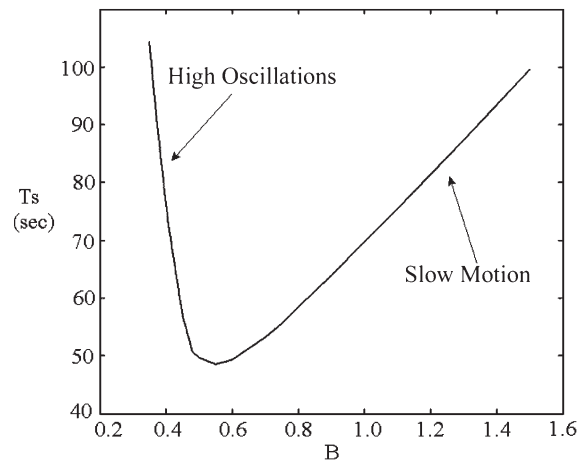
Fig. 7. T_S versus B for linear damping.

The T_S versus the coefficient of damping profile is important. It determines the ability to tune the controller so that the specifications are met. In tuning the controller, there are two requirements. 1) It is required that the maximum spatial deviation (δ_m) between the kinematic and the dynamic path be as small as possible so that the constraints are upheld. 2) It is also required that the settling time be as small as possible. The first requirement
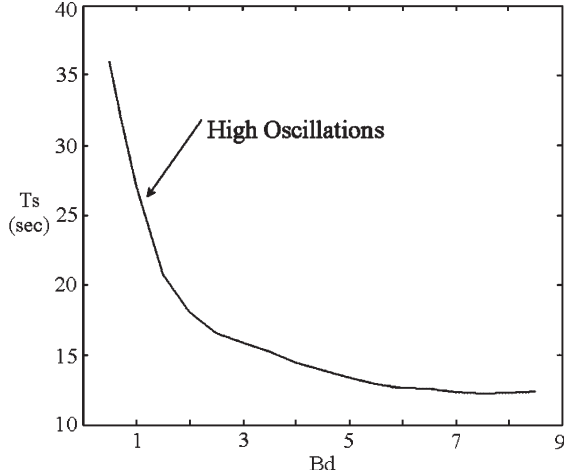
Fig. 8. Settling time versus NADF coefficient.

is achieved by making the coefficient of damping high enough. In the linear viscous damping case, one can only strike a compromise between T_S and δ_m. For the NADF case, this compromise is not needed because both T_S and δ_m are strictly decreasing as a function of B_d.

IV. NONHOLONOMIC CASE

The HPF approach has properties that enable it to plan motion for a nonholonomic system. In the following, methods are outlined on how to adapt the HPF approach to work with nonholonomic robots to generate both kinematic and dynamic trajectories.

A. Model of a Differential Drive Robot

The equation of motion of a nonholonomic mobile robot may be written as

$$\begin{bmatrix} \dot{x} \\ \dot{y} \\ \dot{\theta} \end{bmatrix} = G(x, y, \theta, \nu, \omega) \tag{5}$$

where x and y are the coordinates of the center point of the robot, θ is its orientation, ν is the set radial speed of the robot, ω is the set angular speed, and G is a nonlinear vector function. At a certain (x, y) point in space, (5) may be linearized as

$$\begin{bmatrix} \dot{x} \\ \dot{y} \\ \dot{\theta} \end{bmatrix} = H(x, y, \theta) \begin{bmatrix} \nu \\ \omega \end{bmatrix} \tag{6}$$

where H is a matrix function. The HPF approach can be directly applied to the robot in its linearized form by considering the set radial speed at a certain point in space to be equal to the magnitude of the gradient guidance field at that point, and the set angular speed may be taken as the angle between the robot's orientation and the orientation of the gradient guidance field

$$\nu = |-\nabla V(x, y)|$$
$$\omega = \arg\left(-\nabla V(x, y)\right) - \theta. \tag{7}$$
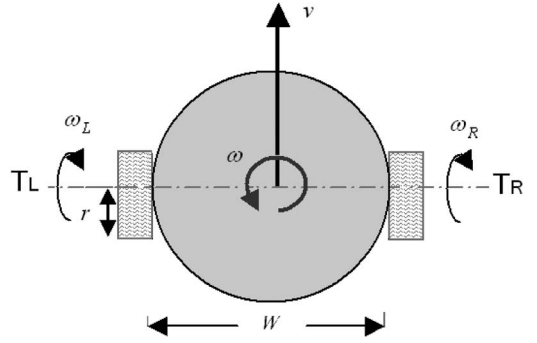
Fig. 9. Differential drive mobile robot.
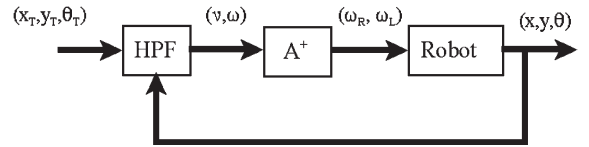
Fig. 10. Kinematic HPF-based planner; nonholonomic case.

The aforementioned procedure can be with little effort adapted to many practical nonholonomic robots. In this paper, planning for a differential drive robot (Fig. 9) is considered.

The equations describing motion for such a robot are as follows:

$$\begin{bmatrix} \dot{x} \\ \dot{y} \\ \dot{\theta} \end{bmatrix} = \begin{bmatrix} \cos(\theta) & 0 \\ \sin(\theta) & 0 \\ 0 & 1 \end{bmatrix} \begin{bmatrix} \nu \\ \omega \end{bmatrix} \tag{8}$$

$$\begin{bmatrix} \nu \\ \omega \end{bmatrix} = \begin{bmatrix} r/2 & r/2 \\ r/W & -r/W \end{bmatrix} \begin{bmatrix} \omega_R \\ \omega_L \end{bmatrix} = A \begin{bmatrix} \omega_R \\ \omega_L \end{bmatrix} \tag{9}$$

where A is the dimension matrix of the robot, r is the radius of the robot's wheels, W is the width of the robot, and ω_R and ω_L are the angular speeds of the right and left wheels of the robot, respectively. The guidance signal derived from the HPF is as follows:

$$\begin{bmatrix} \omega_R \\ \omega_L \end{bmatrix} = A^+ \begin{bmatrix} |-\nabla V| \\ \arg(-\nabla V) - \theta \end{bmatrix} \tag{10}$$

where A^+ is the pseudoinverse of A. For a differential drive robot, $A^+ = A^{-1}$. The block diagram of the HPF planner for the kinematic case is shown in Fig. 10.

The aforementioned scheme is tested for the gradient guidance field in Fig. 11. This field encodes the simple behavior of move right and stay at the center of the road ($y = 0$).

The trajectory corresponding to $\pi/2$ initial orientation is shown in Fig. 12.

B. Dynamic Nonholonomic HPF-Based Planner

As mentioned earlier, a control signal has to be provided to the robot in order to actuate motion. As demonstrated in the holonomic case, using the kinematic HPF-based planner as the HLC in an HLC–LLC setting may be problematic. Aside from the problem of transients, a robustness problem may appear. If wheel slip occurs, the planner will guide the robot based on
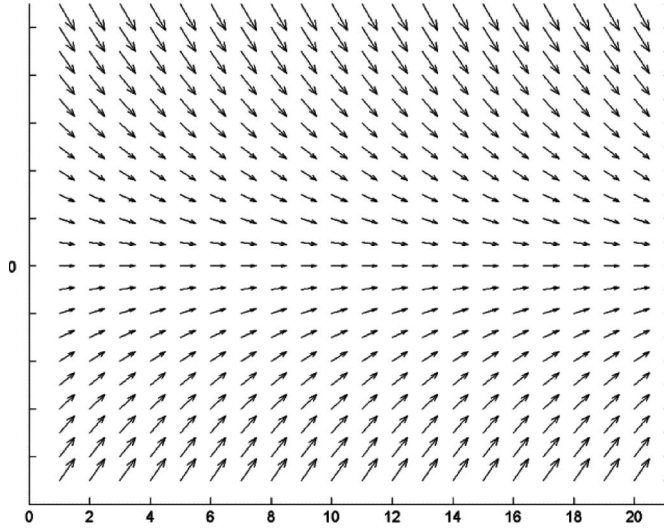
Fig. 11. Move-right-and-stay-at-center gradient guidance field.
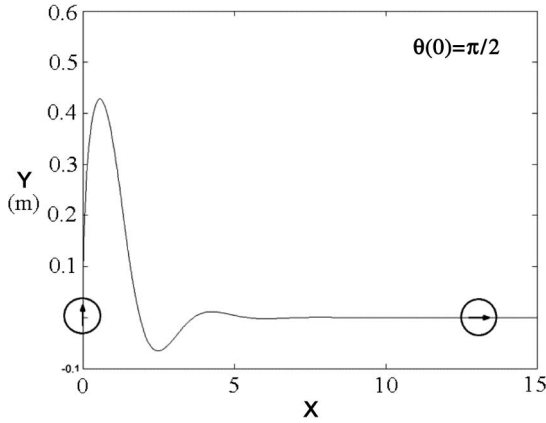
Fig. 12. Trajectories from the nonholonomic kinematic HPF planner.

false information. In this case, problems will arise even if the planner and the controller are functioning properly. Whereas countermeasures against this scenario may be implemented, a planning effort that is less susceptible to this type of problems may be derived by making the planner directly dependent on the torques applied to each wheel. If slip occurs, the torque of a wheel will drop to zero regardless whether the speed of the wheel changes or not. In this section, the idea of NADF is adapted to the nonholonomic case.

The dynamic behavior of the differential drive robot that ties the torques applied to the right and left wheels (T_R, T_L) to the position and orientation of the robot may be described using two coupled differential equations. The first one is obtained by differentiating (8) with respect to time

$$\begin{bmatrix} \ddot{x} \\ \ddot{y} \\ \theta \end{bmatrix} = \begin{bmatrix} \cos(\theta) & 0 \\ \sin(\theta) & 0 \\ 0 & 1 \end{bmatrix} \begin{bmatrix} \dot{\nu} \\ \dot{\omega} \end{bmatrix} + \begin{bmatrix} -\sin(\theta)\dot{\theta} & 0 \\ \cos(\theta)\dot{\theta} & 0 \\ 0 & 0 \end{bmatrix} \begin{bmatrix} \nu \\ \omega \end{bmatrix} \quad (11)$$

the second is derived using Lagrange dynamics in the natural coordinates of the robot

$$\begin{bmatrix} \dot{\nu} \\ \dot{\omega} \end{bmatrix} = \frac{1}{M} \begin{bmatrix} 1/r & 1/r \\ -4r/W^3 & 4r/W^3 \end{bmatrix} \begin{bmatrix} T_R \\ T_L \end{bmatrix} = B \begin{bmatrix} T_R \\ T_L \end{bmatrix} \quad (12)$$
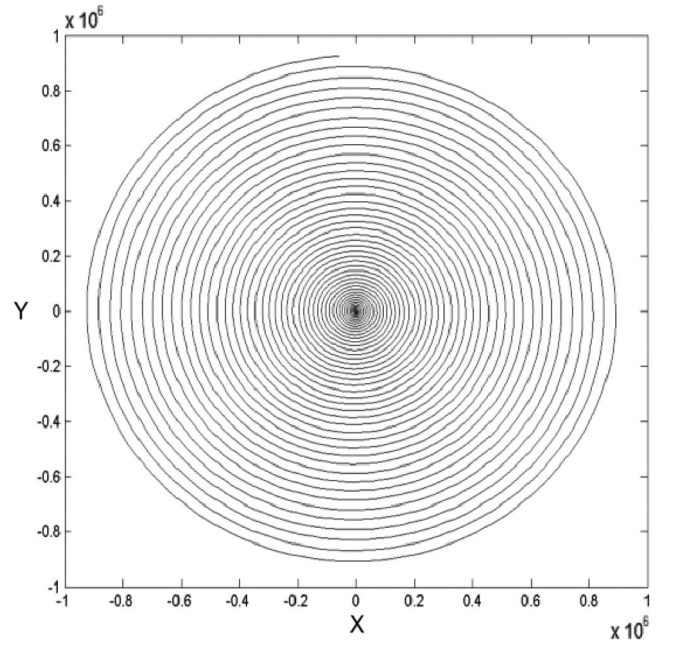
Fig. 13. Adding mass causes instability.
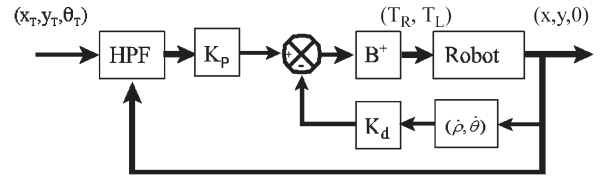
Fig. 14. Dynamic HPF-based planner with linear damping; nonholonomic case.

where M is the mass of the robot. Using $M = 1$, the dynamic model of the robot is used instead of the kinematic model in the example shown in Fig. 12 for the case of $\theta(0) = \pi/2$. As expected, the direct use of the guidance force as a control signal will fail (Fig. 13).

To stabilize the system, an omnidirectional linear viscous damping force applied in the natural coordinates of the robot is used to generate the control signal

$$\begin{bmatrix} T_R \\ T_L \end{bmatrix} = B^+ \left[K_P \cdot \begin{bmatrix} |-\nabla V| \\ \arg(-\nabla V) - \theta \end{bmatrix} - K_d \cdot \begin{bmatrix} \dot{\rho} \\ \dot{\theta} \end{bmatrix} \right] \quad (13)$$

where K_P and K_D are positive constants, B^+ is the pseudoinverse of B, and $\dot{\rho}$ is the radial speed of the robot

$$\dot{\rho} = \sqrt{\dot{x} + \dot{y}}. \quad (14)$$

The block diagram of the planner is shown in Fig. 14.

The response of the system is shown in Fig. 15. As can be seen, the use of rate feedback in the natural coordinates of the robot did stabilize the response and made the system yield to the guidance signal derived from the HPF. Significant transients are observed for a small coefficient of rate feedback. Although increasing this coefficient reduces the transients, it results in reducing the speed of the robot.

One way to sensitize the damping to the guidance signal is to notice that changing the speed of the robot is not needed if the
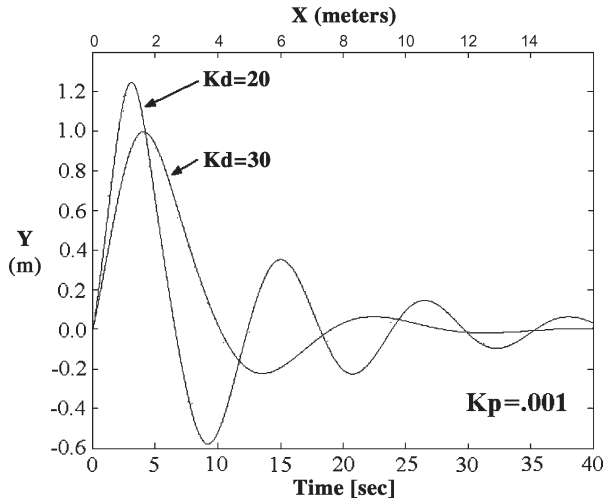
Fig. 15.   Response of the planner in (13).
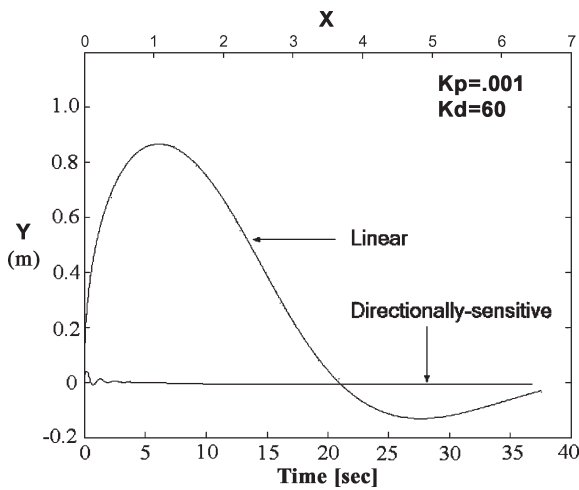
Fig. 16.   Response of the planner in (15) compared with the one in (13).

Fig. 17.   Response of the planner in (15) compared with the one in (16).
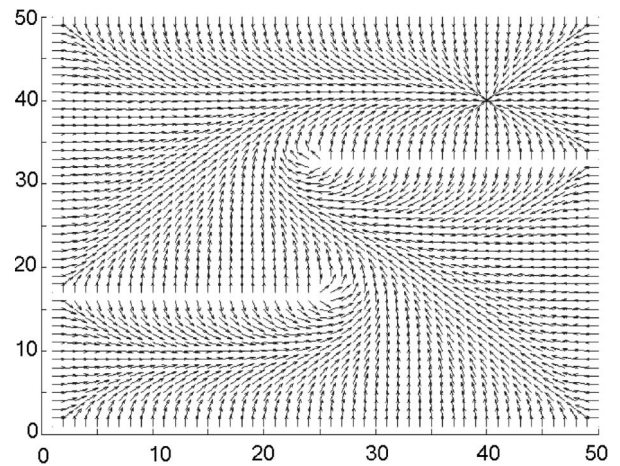
Fig. 18.   Guidance field of a kinematic HPF planner.

actual speed of the system is equal to the reference speed. This leads to a simple, nevertheless effective, change in the form of the control signal

$$
\begin{bmatrix} T_R \\ T_L \end{bmatrix} = B^+ \left[K_P \begin{bmatrix} |-\nabla V| \\ 0 \end{bmatrix} - K_d \begin{bmatrix} \dot{\rho} \\ \dot{\theta} \left(\arg(-\nabla V) - \theta \right) \end{bmatrix} \right].
\tag{15}
$$

In Fig. 16, the direction sensitive damping is compared to the linear damping case using the same coefficients for the planner. As can be seen, sensitizing the damping to direction significantly reduced the overshoot and settling time without compromising the speed of the robot.

The performance can still be further enhanced by making the reference radial speed at a certain point dependent on the orientation of the robot relative to the orientation of the guidance vector. The reasoning that may be used is as follows: if the two orientations are the same, use maximum reference speed. If the two orientations are at right angle, use zero reference speed, and if the two orientations are diametrically opposite, use a negative maximum reference speed. This reasoning may be implemented by simply multiplying the reference speed with cosine of the

difference between the two orientations. The control signal that realizes the aforementioned reasoning is as follows:

$$
\begin{bmatrix} T_R \\ T_L \end{bmatrix} = B^+ \left[K_P \cdot \begin{bmatrix} |-\nabla V| \cdot \cos\left(\arg(-\nabla V) - \theta\right) \\ 0 \end{bmatrix} \right.
$$
$$
\left. -K_d \cdot \begin{bmatrix} \dot{\rho} \\ \dot{\theta}\left(\arg(-\nabla V) - \theta\right) \end{bmatrix} \right].
\tag{16}
$$

In Fig. 17, the direction sensitive controller in (15) is compared to the jointly sensitized controller in (16). As can be seen, the jointly sensitive controller leads to more reduction in the overshoot. Using a $K_p = 0.001$ and a $K_d = 60$, the controller in (16) is tested in a cluttered environment. Fig. 18 shows the harmonic gradient guidance field that is used to motivate the motion of the robot and the holonomic kinematic trajectory such a field generates. Fig. 19 shows the dynamic trajectory that the controller generates and the orientation of the robot as a function of time. It is observed that the nonholonomic dynamic trajectory is very close in shape to the holonomic kinematic trajectory with a satisfactorily smooth orientation profile. The well-behaved control torques applied to the right and left wheels of the robot are shown in Fig. 20.

It was proven in [20] that the gradient dynamical system in (2), which is constructed from an underlying harmonic
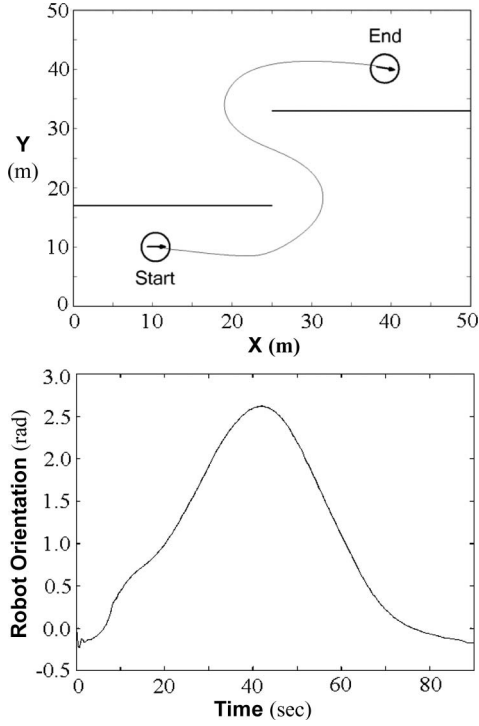
Fig. 19.   Trajectory and curvature using the planner in (16) and the guidance field in Fig. 18.
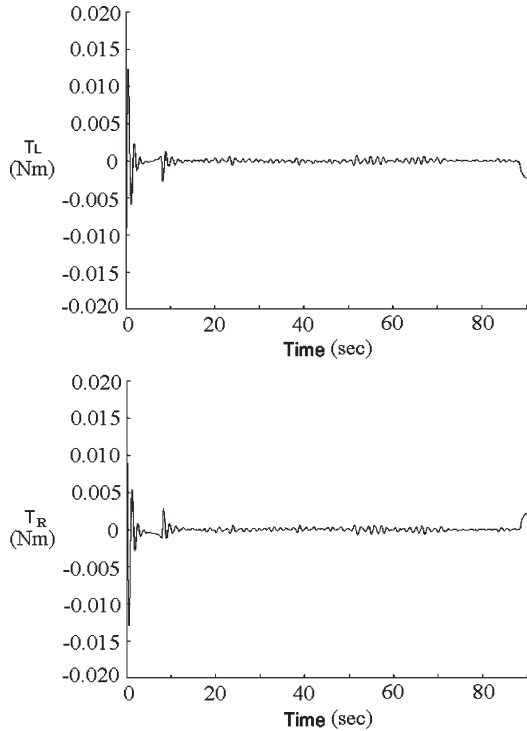
Fig. 20.   Torque control signals corresponding to Fig. 19.

potential, guarantees convergence from any point in Ω to a specified target point. The proof makes use of the fact that a harmonic potential is also a Lyapunov function candidate. The following proposition shows that the procedure suggested in (16) makes it possible for the dynamical system in (2) to steer a differential drive robot with second-order dynamics from

any initial position and orientation in Ω to the target position and orientation encoded in the harmonic field V. A variant of Lyapunov method, called the LaSalle invariance principle [26], is used in the proof.

Propositon 1: The control law in (16) applied to a differential drive robot with second order dynamics described by the system equation in (11) and (12) guarantees global asymptotic convergence of the robot from any initial position and orientation in Ω to the target potion point (x_T, y_T) and orientation $(\arg(-\nabla V \ (x_T, y_T))$ encoded in the harmonic potential V provided that $K_p > 0$ and $K_d > 0$.

Proof: Consider the following Lyapunov function candidate:

$$\Xi = K_P \cdot M \cdot V(x, y) + \frac{1}{2} K_d \cdot I \cdot (\arg(-\nabla V(x, y) - \theta)^2$$

$$+ \frac{1}{2} I \cdot \dot{\theta}^2 + \frac{1}{2} M \cdot \dot{\rho}^2 \quad (17)$$

where M is the mass of the robot, I is its inertia, and K_p and K_d are positive constants. Notice that $V(x, y)$ is a valid Lyapunov function [20]. It is always positive except at the target point (x_T, y_T), where it is equal to zero. As a result, Ξ is always positive except at the target position and orientation, when the robot is at a standstill. The time derivative of Ξ is as follows:

$$\dot{\Xi} = K_P \cdot M \cdot \nabla V(x, y)^t \begin{bmatrix} \dot{x} \\ \dot{y} \end{bmatrix} - K_d \cdot I \cdot \dot{\theta} \cdot (\arg(-\nabla V(x, y) - \theta)$$

$$+ I \cdot \dot{\theta} \cdot \ddot{\theta} + M \cdot \dot{\rho} \cdot \ddot{\rho}. \quad (18)$$

Notice that

$$\nabla V(x, y) = |\nabla V(x, y)| \begin{bmatrix} \cos(\arg(-\nabla V(x, y) + \pi)) \\ \sin(\arg(-\nabla V(x, y) + \pi)) \end{bmatrix} \quad (19)$$

$$\begin{bmatrix} \dot{x} \\ \dot{y} \end{bmatrix} = \dot{\rho} \begin{bmatrix} \cos(\theta) \\ \sin(\theta) \end{bmatrix}. \quad (20)$$

Substituting (12), (16), (19), and (20) in (18) and noticing that, for a differential drive robot $B^+ = B^{-1}$, we have

$$\dot{\Xi} = -K_P \cdot M \cdot \dot{\rho} \cdot |\nabla V(x, y)| \cdot \cos(\arg(-\nabla V(x, y)) - \theta)$$

$$- K_d \cdot I \cdot \dot{\theta} \cdot (\arg(-\nabla V(x, y)) - \theta) - K_d \cdot I \cdot \dot{\theta}^2$$

$$- K_P \cdot M \cdot \dot{\rho}^2 + K_d \cdot I \cdot \dot{\theta} \cdot (\arg(-\nabla V(x, y)) - \theta)$$

$$+ K_P \cdot M \cdot \dot{\rho} \cdot |\nabla V(x, y)| \cdot \cos(\arg(-\nabla V(x, y)) - \theta).$$

$$(21)$$

Therefore,

$$\dot{\Xi} = -K_d \cdot I \cdot \dot{\theta}^2 - K_p \cdot M \cdot \dot{\rho}^2. \quad (22)$$

As can be seen, the time derivative of the Lyapunov function is negative semidefinite. According to the LaSalle principle, motion will converge to a subset of the set of points (E) for which the time derivative of Ξ is zero

$$E = \{\dot{\rho} = 0, \dot{\theta} = 0, x, y, \theta\}. \quad (23)$$

The subset is called the minimum invariant set (S) and may be computed as the set of point for which is the gradient dynamical system in (2). It was shown in [20] that motion for (2) is guaranteed to converge to the target point x_T, y_T; hence, the orientation of the robot will converge to $\arg(-\nabla V(x_T, y_T))$. In other words, the dynamical differential drive robot will converge to set

$$S = \left\{ \dot{\rho} = 0, \dot{\theta} = 0, x = x_T, y = y_T, \theta = \arg\left(-\nabla V(x_T, y_T)\right) \right\} \tag{24}$$

provided that K_p and K_d are positive.

V. CONCLUSION

In this paper, the HPF motion planning method is cast in a navigation control framework where *a priori* data about a situation are directly converted into a control signal. The gradient of an HPF, which can only provide a guiding reference, is converted into a control signal using the NADF concept suggested in this paper. As was demonstrated, attempting to convert the gradient field into a control signal by adding a linear viscous damping force (a force proportional to velocity) may be problematic. On the other hand, carrying out such an extension using the NADF approach is straightforward and practical. This is because the NADF approach is developed to take into consideration that the dual role of the gradient field of an HPF plays both as a control signal and a guidance provider. The simultaneous consideration of these two factors is what enables the control signal to effectively suppress transients without slowing down motion. The work in this paper may be considered as another step toward the HPF approach attaining its full potential.

REFERENCES

[1] C.-L. Hwang, L.-J. Chang, and Y.-S. Yu, "Network-based fuzzy decentralized sliding-mode control for car-like mobile robots," *IEEE Trans. Ind. Electron.*, vol. 54, no. 1, pp. 574–585, Feb. 2007.
[2] X.-L. Wei, J. Wang, and Z.-X. Yang, "Robust smooth-trajectory control of nonlinear servo systems based on neural networks," *IEEE Trans. Ind. Electron.*, vol. 54, no. 1, pp. 208–217, Feb. 2007.
[3] Y. Tipsuwan and M.-Y. Chow, "Gain scheduler middleware: A methodology to enable existing controllers for networked control and teleoperation—Part I: Networked control," *IEEE Trans. Ind. Electron.*, vol. 51, no. 6, pp. 1218–1227, Dec. 2004.
[4] S. Kim and F. C. Park, "Fast robot motion generation using principal components: Framework and algorithms," *IEEE Trans. Ind. Electron.*, vol. 55, no. 6, pp. 2506–2516, Mar. 2008.
[5] J. Schwartz and M. Sharir, "A survey of motion planning and related geometric algorithms," *Artif. Intell.*, vol. 37, no. 1–3, pp. 157–169, Dec. 1988.
[6] Y. Hwang and N. Ahuja, "Gross motion planning," *ACM Comput. Surv.*, vol. 24, no. 3, pp. 219–291, Sep. 1992.
[7] R. Aggarwal and G. Leitmann, "A maxmin distance problem," *Trans. ASME, J. Dyn. Syst., Meas. Control*, vol. 94, no. 2, pp. 155–158, Jun. 1972.
[8] G. Leitmann and J. Skowronski, "Avoidance control," *J. Optim. Theory Appl.*, vol. 23, no. 4, pp. 581–591, Dec. 1977.
[9] W. Schmitendorf, B. Barmish, and B. Elenbogen, "Guaranteed avoidance control and holding control," *Trans. ASME, J. Dyn. Syst. Meas. Control*, vol. 104, pp. 166–172, Jun. 1982.
[10] S. Masoud and A. Masoud, "Constrained motion control using vector potential fields," *IEEE Trans. Syst., Man, Cybern. A, Syst., Humans*, vol. 30, no. 3, pp. 251–272, May 2000.
[11] C. Langton, "Artificial life," in *Artificial Life SFI Studies in the Science of Complexity*, C. Langton, Ed. Reading, MA: Addison-Wesley, 1988, pp. 1–47.
[12] O. Khatib, "Real-time obstacle avoidance for manipulators and mobile robots," in *Proc. IEEE Int. Conf. Robot. Autom.*, St. Louis, MO, Mar. 25–28, 1985, pp. 500–505.
[13] C. Connolly, R. Weiss, and J. Burns, "Path planning using Laplace equation," in *Proc. IEEE Int. Conf. Robot. Autom.*, Cincinnati, OH, May 13–18, 1990, pp. 2102–2106.
[14] E. Prassler, "Electrical networks and a connectionist approach to pathfinding," in *Connectionism in Perspective*, R. Pfeifer, Z. Schreter, F. Fogelman, and L. Steels, Eds. Amsterdam, The Netherlands: Elsevier, 1988.
[15] I. Tarassenko and A. Blake, "Analogue computation of collision-free paths," in *Proc. IEEE Int. Conf. Robot. Autom.*, Sacramento, CA, Apr. 1991, pp. 540–545.
[16] J. Decuyper and D. Keymeulen, "A reactive robot navigation system based on a fluid dynamics metaphor," in *Proc. 1st Workshop Parallel Problem Solving From Nature*, H. Schwefel and R. Hartmanis, Eds., Dortmund, Germany, Oct. 1–3, 1990, pp. 356–362.
[17] K. Sato, "Collision avoidance in multi-dimensional space using Laplace potential," in *Proc. 15th Conf. Robot. Soc. Jpn.*, 1987, pp. 155–156.
[18] A. Masoud and S. Masoud, "Evolutionary action maps for navigating a robot in an unknown, multidimensional, stationary environment, Part II: Implementation and results," in *Proc. IEEE Int. Conf. Robot. Autom.*, Albuquerque, NM, Apr. 21–27, 1997, pp. 2090–2096.
[19] A. Masoud and S. Masoud, "Robot navigation using a pressure generated mechanical stress field, the biharmonic potential approach," in *Proc. IEEE Int. Conf. Robot. Autom.*, San Diego, CA, May 8–13, 1994, pp. 124–129.
[20] S. Masoud and A. A. Masoud, "Motion planning in the presence of directional and regional avoidance constraints using nonlinear, anisotropic, harmonic potential fields: A physical metaphor," *IEEE Trans. Syst., Man, Cybern. A, Syst., Humans*, vol. 32, no. 6, pp. 705–723, Nov. 2002.
[21] S. Axler, P. Bourdon, and W. Ramey, *Harmonic Function Theory*. New York: Springer-Verlag, 1992.
[22] K. Althofer, D. Fraser, and G. Bugmann, "Rapid path planning for robotic manipulators using an emulated resistive grid," *Electron. Lett.*, vol. 31, no. 22, pp. 1960–1961, Oct. 26, 1995.
[23] M. Stan, W. Burleson, C. Connolly, and R. Grupen, "Analog VLSI for robot path planning," *Analog Integr. Circuits Signal Process.*, vol. 6, no. 1, pp. 61–73, Jul. 1994.
[24] D. Koditschek, "Exact robot navigation by means of potential functions: Some topological considerations," in *Proc. IEEE Int. Conf. Robot. Autom.*, Raleigh, NC, Mar. 1987, pp. 1–6.
[25] D. Koditschek and E. Rimon, "Exact robot navigation using artificial potential functions," *IEEE Trans. Robot. Autom.*, vol. 8, no. 5, pp. 501–518, Oct. 1992.
[26] J. LaSalle, "Some extensions of Lyapunov's second method," *IRE Trans. Circuit Theory*, vol. CT-7, no. 4, pp. 520–527, Dec. 1960.
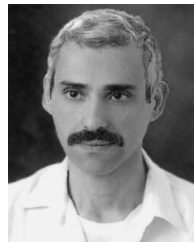
Ahmad A. Masoud (M'83) received the B.Sc. degree in electrical engineering, with a major in power systems and a minor in communication systems, from Yarmouk University, Irbid, Jordan, in 1985, and the M.Sc. (digital signal processing) and Ph.D. (robotics and autonomous systems) degrees in electrical engineering from Queen's University, Kingston, ON, Canada, in 1989 and 1995, respectively.

He was a Researcher with the Electrical Engineering Department, Jordan University of Science and Technology, Irbid, Jordan, from 1985 to 1987. He was also a Part-Time Assistant Professor and a Research Fellow with the Electrical Engineering Department, Royal Military College of Canada, Kingston, from 1996 to 1998. During that time, he carried out research in digital-signal-processing-based demodulator design for high-density multiuser satellite systems and taught courses in robotics and control systems. He is currently an Assistant Professor with the Electrical Engineering Department, King Fahd University of Petroleum and Minerals, Dhahran, Saudi Arabia. His current interests include navigation and motion planning, robotics, constrained motion control, intelligent control, and DSP applications in machine vision and communication.